Published in final edited form as:
Cell Commun Adhes. 2013 February ; 20(0): . doi:10.3109/15419061.2013.775256.

A History of Gap Junction Structure: Hexagonal Arrays to Atomic Resolution

Rosslyn Grosely and **Paul L. Sorgen**
Department of Biochemistry and Molecular Biology, University of Nebraska Medical Center, Omaha, NE, USA

Abstract

Gap junctions are specialized membrane structures that provide an intercellular pathway for the propagation and/or amplification of signaling cascades responsible for impulse propagation, cell growth, and development. Prior to the identification of the proteins that comprise gap junctions, elucidation of channel structure began with initial observations of a hexagonal nexus connecting apposed cellular membranes. Concomitant with technological advancements spanning over 50 years, atomic resolution structures are now available detailing channel architecture and the cytoplasmic domains that have helped to define mechanisms governing the regulation of gap junctions. Highlighted in this review are the seminal structural studies that have led to our current understanding of gap junction biology.

Keywords

Review; gap junction structure; biophysical techniques

GAP JUNCTION STRUCTURE: LOW RESOLUTION

Determination of protein structure is typically undertaken to explicate the molecular mechanism(s) of protein function. However, unique to the gap junction, structural characterization began several years prior to the protein being identified. In 1958, an electron micrograph (EM) of cardiomyocyte plasma membranes revealed specialized regions between adjacent cells that appeared as a five-layered, single, dense lamina (Sjostrand et al., 1958). The tight apposition, or nexus, was also present in striated and smooth muscle cells and was believed to be involved in electrical conduction (Karrer, 1960; Dewey & Barr, 1962). Similarly, EMs of the synaptic membrane complex from Mauthner cell dendrites revealed sectional disk-like structures. The disks were formed by tight apposition of the pre- and post-synaptic membranes, which occluded the typical 100–200 Å intermembrane gap. Hexagonal arrays of 90 Å /unit were apparent from a frontal view, with each unit containing a central dense spot of <25 Å, and an 85 Å repetitive bead-like pattern in transverse sections of the discs (Robertson, 1963, 1961). Thickness of the disks was ~125 Å suggesting that the structures were due to a tight, intermembrane apposition rather than membrane fusion. Similar membrane morphological features were identified and shown to correlate with electrical transmission between teleost spinal neurons (Bennett et al., 1963). The apparent prevalence of the hexagonal nexus structures led to the hypothesis of an

Address correspondence to Dr. Paul Sorgen, UNMC, Biochemistry and Molecular Biology, 985870 Nebraska Med Ctr., Omaha, NE 68198-5870, USA. Phone: +(402) 559-7557. Fax: +(402) 559-6650. psorgen@unmc.edu.

Declaration of interest: The authors report no declarations of interest. The authors alone are responsible for the content and writing of the paper.

analogous particle in all membrane systems (Fernandez Moran et al., 1964). However, lipid micelles had previously been shown to organize into a hexagonal arrangement at elevated temperatures (Stoeckenius, 1962). The possibility existed that the hexagonal array of the nexus was simply due to a phospholipid phase transition (Benedetti & Emmelot, 1965); therefore, to determine if the hexagonal array was an artifact of sample preparation, rat liver plasma membranes were compared at 2°C and 37°C (Benedetti & Emmelot, 1965). Nexus structures were only observed at 37°C indicating that nexus formation may be an artifact of temperature. Alternatively, it was proposed that stabilization rather than formation of the nexus was temperature dependent, given that pretreatment of the isolated membranes with H_2O before fixation and staining did not further promote phospholipid phase transition and nexus formation. Substantiation of the latter hypothesis arose upon discovery of two characteristically discrete types of intercellular junctions in the nexus.

In 1963, Farquhar and Palade (1963) surveyed EMs of epithelia cells providing identification of the zonula occludens (tight junctions), zonula adherens, and the macula adherens. However, until the work of Revel and Karnovsky (1967), the nexus structure or ‘gap junction’ (GJ; Figure 1A) was not delineated from the tight junctions. EM samples were prepared with Lanthanum salts in the fixative solution. Lanthanum, which is electron opaque, diffused throughout the accessible extracellular space revealing characteristics typical of zonula occludens, zonula adherens, and macula adherens; however, there were also regions of close apposition between neighboring cells. Cross-sections through this region appeared as a five-layered, single dense lamina. The midline was electron opaque and thick indicating the presence of the extracellular tracer molecule unlike the midline of true tight junctions, which was weak and thin due to occlusion of lanthanum. Treatment of the samples with uranyl acetate instead of lanthanum established the presence of an 18 Å gap (Figure 1B) between the outer leaflets of the apposed membranes. The GJs exhibited the same structural features and dimensions previously characterized by Robertson (1961, 1963). The presence of a dense spot at the center of each unit suggested that GJs were hollow structures with hydrophilic characteristics. Revel and Karnovsky (1967) acknowledged that GJs were located in areas associated with intracellular conduction and might possibly allow for permeation of larger molecules.

Intercellular transfer of molecules involved in regulating cell growth was a suspected function of GJs, but because specific cellular growth signals were yet to be identified, the ability to test this hypothesis was limited. However, using a simple but elegant experimental design, in which the membrane resistance of normal hepatic cells was compared to that of junctionally deficient hepatic cancer cells, Loewenstein and Kanno (1966) provided indirect evidence that regulation of cell growth was dependent upon GJs. The lack of growth regulation typical of cancer cells was implied to be a result of the inability to transfer control signals via GJs. A more direct approach was used by Payton et al. (1969) to demonstrate molecular permeability through GJs at the axo-ganglia interface of apposed crayfish septate axons. A microelectrode filled with Procion yellow M4RS (membrane impermeable; 500 Da) was inserted distal to the axon septum and concomitantly injected dye and stimulated hypopolarization. A second electrode filled with KCl located on the other side of the septum measured the electrical propagation at the synapse. Microscopic observation of the cells indicated intercellular transfer of Procion yellow M4RS via direct cytoplasm-to-cytoplasm exchange.

Detergent fractionation of isolated plasma membranes was used to obtain a pellet containing tight junctions (Benedetti & Emmelot, 1968). However, EM ultrastructure of the pellet was similar to junctions previously defined as GJs (Revel & Karnovsky, 1967). The characteristic gap was not apparent in the EMs of the junctions, which casted some doubt as to whether the junctions were of the gap type. In thin sections of negatively stained

preparations, the membrane appeared as two layers of globules. It was suggested that the globules and hexagonal units might be the same structure and likely composed of hydrophobic proteins with a central, hydrophilic hole. In areas where the membrane was torn, the sheets appeared to be composed of two identical layers. In a subsequent EM study, freeze fracture was used to split the lipid bilayer into a cytoplasmic and an extracellular surface revealing a tightly packed hexagonal array with a complementary particle and pit on each face (McNutt & Weinstein, 1970). The extracellular pit diameter was 30–40 Å (Figure 1B), but the cytoplasmic diameter was below the resolution limits. The results suggested that the nexus is composed of macromolecular structures that formed intercellular channels.

Goodenough and Stoeckenius (1972) further characterized the molecular components of the GJs, using chromatography and electrophoresis. The GJ plaques consisted of phosphatidylcholine, phosphatidylethanolamine, and a ~20 kDa protein. The compositional simplicity of the GJs, as compared to a non-junctional membrane, was also supported by low-angle X-ray diffraction data (Goodenough & Stoeckenius, 1972). Using known information about the morphological dimensions of GJs, expected diffraction maxima were back calculated and compared to the observed diffraction maxima. The observed values were consistent with a GJ thickness of 150 Å and subunit center-to-center spacing of 86 Å (Figure 1B). To enable more rigorous structural analysis, ~1–5 mg of intact GJs suitable for structural and biochemical analysis was obtained using a bulk purification protocol (Goodenough, 1974). Freeze-fracture specimens revealed that the GJs extended from cytoplasm face to cytoplasm face with the hexagonal subunits, or ‘connexons’ (Figure 1C), embedded in the apposed lipid bilayers (Goodenough, 1975).

GAP JUNCTION STRUCTURE: MEDIUM RESOLUTION

Mouse hepatic connexons were analyzed by SDS-PAGE in the absence and presence of disulfide reducing agents (Goodenough, 1974). The electrophoretic profile under non-reducing conditions contained two major bands, with molecular weights of 34 and 18 kDa, and two minor bands, which migrated as a doublet at ~10 kDa. Under reducing conditions, both the major bands collapsed to the 10 kDa doublet. At the time, the results were believed to indicate that connexons were composed of two disulfide-linked peptides called ‘connexins’ (Figure 1D; Goodenough, 1974). Trypsin digestion of the GJs did not alter connexon ultrastructure, but led to the formation of GJ-containing vesicles which were 0.5–0.9 mm in diameter (Goodenough, 1976). Curvature of the vesicles caused poor diffraction quality, but was regarded as a potential system for future functional assays (Makowski et al., 1977; Caspar et al., 1977).

In a collaboration between the Goodenough and Caspar labs, X-ray diffraction data were related to morphological features observed in EMs of hepatic GJs (Caspar et al., 1977) and the arrangement of the chemical components within the GJ channels was determined; H_2O, lipids, and proteins have distinct diffraction patterns (Makowski et al., 1977). Diffraction patterns from purified GJs prior to being processed for EM were consistent with data collected post-processing, indicating that packing of connexons into a hexagonal array was not an artifact of sample preparation (Caspar et al., 1977). Diffraction intensities decreased at the center suggesting short-range disorder in the connexon lattice. Perfusion of mouse livers with sucrose decreased short-range disorder allowing continuity in the lattice between the extracellular and cytoplasmic faces seen in EMs of freeze fracture samples. The strong diffraction points at 30 Å were indicated as lipids. The lattice retained long range-order, with an average unit spacing of 80–90 Å. The dimensions were used to estimate that the channel occupies 190,000 $Å^3$. Based on a molecular weight of 20–30 kDa, each connexon was composed of 4–8 polypeptides. The hexagonal lattice implies that six nearest-neighbor interactions are required for stabilization. With this in mind, connexons were suggested to

have a hexameric structure. Of importance, in addition to furthering our understanding of GJ structure, the work by Caspar, Makowski, and Phillips was a significant breakthrough in the field of crystallography, as there were no sophisticated modeling techniques for data interpretation available at the time.

In a later study, two distinct forms of connexons were identified (Zampighi & Unwin, 1979). Form B was obtained by dialyzing Form A against water. Peak broadening in the EMs collected for Form B suggested these connexons to be less ordered. Peak amplitudes and phases computed by Fourier transformation indicated six-fold symmetry within the membrane plane and two-fold symmetry across the junction. There was little variation among each form, but there were notable diffraction differences between Forms A and B. SDS-PAGE analysis indicated that proteins from both forms have the same molecular weight, suggesting that the differences were due to structural variation. Additionally, returning Form B to a lipid environment reverted the connexons to Form A further indicating that the differences were due to molecular rearrangements. Diffraction data indicated radial and tangential displacement about the connexon six-fold axis in Form B relative to Form A, which resulted in a decrease of subunit tilt from 14° to 9° and a 23° rotation of the connexons in the lattice. The rearrangement moved density toward the central opening of the connexon, suggesting a potential mechanism for regulating GJ intercellular communication (GJIC).

To determine if similar structural changes occur under physiological conditions, projection maps were generated from X-ray diffraction data of hepatic connexons dialyzed against a buffer containing Ca^{+2} or Ca^{+2} and EGTA (Unwin & Ennis, 1984). Ca^{2+} was chosen based on results from a previous study by Peracchia and Dulhunty (1976) on septate lateral giant axons of crayfish. Electrical recordings and thin section microscopy indicated concomitant cellular decoupling and conformational changes in septate GJs in response to free Ca^{+2}. The effects were reversed upon perfusion with EDTA. In the study by Unwin and Ennis (1984), Ca^{+2} induced a change in the radial and tangential alignment of the connexon subunits relative to the six-fold axis by 7.5° compared to connexons with EGTA-chelated Ca^{+2}. The change in tilt is facilitated by connexon subunits sliding along established lines of contact, as no rotation was observed about the axes of the individual connexon rods. Ca^{+2}-induced relaxation of the left-handed twist of the connexons produced a widening of the extracellular face and a narrowing of the cytoplasmic opening by ~18 Å. Although details of the precise mechanism were unclear, the authors suggested that Ca^{+2} may regulate GJIC by causing a conformational change at one face of the connexon that propagates to the opposite face of the connexon.

In 1985, Edman degradation was utilized to sequence liver and heart GJ proteins and identified that they were distinct but related (Nicholson et al., 1985). Cloning and characterization of rat and human liver GJ cDNA resulted in the identification of a 32 kDa protein (Kumar & Gilula, 1986; Paul, 1986). Later, Northern analysis of rat heart cDNA was used to characterize a GJ protein with a molecular mass of 43 kDa (Beyer et al., 1987). Similar experiments were used to identify other connexin isoforms and demonstrate tissue-specific expression profiles for each. Gimlich et al. (1990) proposed a nomenclature system based on tissue expression where liver connexins Cx32 and Cx26 would be named β1 and β2, respectively, and the cardiac connexin Cx43 would be α1. Because multiple connexins were present in each tissue, a naming system based on isoform molecular weight was preferred (Beyer et al., 1987). Hydropathy plots predicted that the connexins have four transmembrane domains (TM1–TM4; Figure 1D). Diffraction and circular dichroism (CD) analysis suggested that the TMs are helical (Tibbitts et al., 1990; Cascio et al., 1990). Proteolysis susceptibility and site-directed antibody localization studies determined that connexins have two extracellular loops (EL1 and EL2) and one cytoplasmic loop (CL). The

amino- (NT) and carboxyl-termini (CT) are also located on the cytoplasmic side (Figure 1D).

Atomic force microscopy (AFM) was used to investigate the structural features of rat hepatic GJs (Hoh et al., 1991). The junctional membranes underwent multiple sweeps of the AFM at low force (1 pN) without loss of structural integrity. The plaques ranged in size from 0.5 to 1.0 μm exhibiting typical shape and membrane distribution. The junctional membrane was 14.4 nm thick and appeared smooth and undulating at high magnification. Increases in force to 15 pN disrupted and then removed the top bilayer exposing the extracellular surface of the apposed connexons. For previous EM and X-ray studies, the splitting required stringent conditions, which potentially disrupt the native structure of the connexons. The relatively mild force required to dissect the paired connexons using the AFM probe presumably did not alter the structural characteristics of the remaining connexon layer. Exposure of the extracellular surface of the plaques revealed a hexagonal array of connexons that protruded 0.4 nm above the membrane surface. A central pit apparent in many of the connexons was attributed to the extracellular pore. The diameter of the extracellular face ranged from 4 to 6 nm, which was larger than that determined previously by EM and X-ray diffraction. Consistently, however, the AFM data indicated that connexons have six-fold symmetry and a center-to-center spacing of 9.1 nm.

At the time of initial connexon characterization, AFM had been commercially available for only two years. With improvements in tip quality and data analysis, substantial sub-structural detail was observed. One factor limiting EM and X-ray image resolution beyond 20 Å was the short-range disorder in the hexagonal array, which was overcome by correlation averaging and Fourier analysis of AFM data (Hoh et al., 1993). AFM images of hepatic connexons resolved to 2.5 nm in the XY plane and 0.2 nm in the Z plane were consistent with previous studies (Hoh et al., 1991; Zampighi & Unwin, 1979; Goodenough, 1976). The connexons exhibited peripheral height modulation on the extracellular face, suggesting that connexon dimerization results from the interdigitation of two surfaces (Hoh et al., 1993).

Using a combination of immunofluorescence and AFM, Lal et al. (1995) characterized cardiac Cx43 GJ plaques. Present in all specimens were plaque clusters with morphologies similar to dissected connexons. The connexons in the ‘hemiplaques,’ like the dissected connexons, were hexagonally arrayed with short-range disorder. The likelihood that the clusters of unpaired connexons were an experimental artifact was low, given that hemiplaques, which ranged from 0.2 to 1 μm^2 in size, accounted for 12–17% of the total junctional area and were present in wet and dried samples. Additionally, antibodies specific to the extracellular domain localized at cardiomyocyte intercalated discs (el Aoumari et al., 1991). Because antibody-binding sites in the extracellular domain are obstructed in whole junctions, the results suggested that not all connexons at the intercalated discs were paired.

GAP JUNCTION STRUCTURE: HIGH RESOLUTION

Channel architecture

In 1999, a groundbreaking study was published, in which the 3D electron crystallographic structure of a CT-truncated Cx43 GJ channel was resolved to 7.5 Å in the membrane plane and 21 Å in the vertical plane (Figure 2A; Unger et al., 1999). Truncation of Cx43 at residue 263 allowed for better crystal packing, which increased the diffraction quality and resolution. Removal of most of the Cx43CT decreased the overall GJ thickness from 250 Å to 150 Å. The outer diameter of the channel narrowed from 70 Å at the cytoplasmic surface to 50 Å in the extracellular portion. A vertical section of the map indicated a similar narrowing of the aqueous pore from 40 Å at the cytoplasmic face to 15 Å at the extracellular

surface. However, the diameter widened to 25 Å within the extracellular vestibule. Contours of electron density in lateral cross-sections through the extracellular region defined the molecular boundaries of the connexon hexamer. In a cross-section through the membrane region, 24 tubular densities were apparent; suggesting that each of the six connexin subunits is composed of four helical TM domains. At the current resolution, assignment of the primary sequence to the structural components was not possible. Therefore, the TM helices were arbitrarily designated as A–D. The helices were packed with a left-handed twist, with the exception of the two pore-lining domains (B/C), which had right-handed packing. The large tilt angle of domain C, which is the primary pore-lining helix, produced the observed narrowing within the channel. Additionally, the helical conformation of domain C extended beyond the boundary of the bilayer into the cytoplasm. In a later study, difference maps were generated using 2D crystals of full-length Cx43 GJ channels in an attempt to visualize the intracellular domains (Cheng et al., 2003). The absence of intracellular electron density supported structural disorder in cytoplasmic domains originally suggested by Makowski et al. (1984).

The response of full-length Cx43 connexons to Ca^{+2} was examined by AFM (Thimm et al., 2005). In Ca^{+2} free buffer, images of the extracellular face exhibited a typical hexameric donut-like structure. The central pore was 2.5 nm in diameter with a depth of 0.8 nm. Ca^{+2} concentrations of 1.4 and 1 mM reduced pore diameter to 1.8 nm in 73% and 26% of the channels, respectively. The conformational response, which was specific to Ca^{+2}, as neither Ni^{+2} nor Mg^{+2} elicited a change, supported a possible mechanism for regulation of GJIC. The open and closed channel diameters were similar to those predicted by EM (Unger et al., 1999). In Cx26 hemi-channels, Ca^{+2} also induced a narrowing of pore diameter; however, the pore in the open and closed state (1.5 and 0.6 nm, respectively) was smaller than Cx43 channels (Muller et al., 2002).

AFM was later used to demonstrate that pH-mediated closure of Cx26 channels occurred through a different mechanism from that of Ca^{+2} (Yu et al., 2007). Cx26 connexons closed in response to acidification, but only in an aminosulfonate buffer. At pH 7.6, the channel entrance diameter was 1.7 nm, and 0.6 nm at pH 6.0. Acidification also decreased pore depth and induced a ~6.5° rotation in the connexon lobes. Collectively, the results hinted that pH-mediated closure involves a physical gate located near the extracellular surface. In a more detailed study, the Sosinsky lab reported the electron crystallographic structure of Cx26 connexons reconstituted in lipid bilayers (Oshima et al., 2007). To improve expression, a M34A substituted construct was used. Although the $Cx26_{M34A}$ was purified as a connexon, the authors hypothesized that the connexons re-docked during the crystallization process forming complete channels. The 3D channel structure was determined at a resolution of 10 Å. Pore dimensions and position of the helices were similar to Cx43 channels (Unger et al., 1999). The similarity in structure between α- and β-type connexins strongly implicates the divergent cytoplasmic domains as mediators of channel regulation among the connexins. Unfortunately, due to their flexibility, the cytoplasmic domains are not resolved. Projection maps of $Cx26_{M34A}$ indicated a plug at the center of the pore to be in direct contact with the inner surface of the vestibule (Oshima et al., 2008). In a later study, improvements in 3D resolution to 5 Å indicated that the Cx26 NT was the most reasonable candidate for the physical blockade (Oshima et al., 2011). Because the NT is the least divergent cytoplasmic domain, the possibility exists that other family members utilize this gating mechanism. However, the $Cx26_{M34A}$ channel has unique physiological properties and may also have an atypical gating mechanism (Oshima et al., 2011). Furthermore, Liu et al. (2006) implicated the CT domain in Ca^{+2}-mediated closure of Cx43 channels. AFM tips modified with antibodies to Cx43 residues G252–G270 or D360-I382 were presented to Cx43 connexons reconstituted in a lipid bilayer. An extension of ~105 nm was detected when Cx43 interacted with anti-$CT_{360–382}$. The anti-$CT_{252–270}$-Cx43 interaction extended

~57 nm, an expected result, given that the site of interaction is in the middle of the CT. Introduction of 1.8 mM Ca^{+2} resulted in a conformation that disrupted antibody recognition of the CT supporting the involvement of the domain in regulating Cx43 channel closure.

The highly anticipated crystal structure of the Cx26 GJ channel was resolved to 3.5 Å (Maeda et al., 2009; Figure 2B). The overall channel architecture was similar to the EM structures of Cx43 and Cx26 (Unger et al., 1999; Oshima et al., 2011). The height was 155 Å, with an outer diameter of 90 Å on the cytoplasmic face that narrowed to 50 Å on the extracellular side. The internal diameter of the channel across the gap was 17 Å. Identification of selenium-labeled Met residues in the NT and disulfide bonds in the extracellular domain facilitated assignment of the TM domains. The inner diameter of the membrane-embedded portion of the connexon pore narrowed from 40 to 14 Å due to a kink in TM1 followed by a 3_{10} helix. TM1 was identified as the primary pore-lining domain, as previously suggested by Verselis et al., 2009, resolving conflicting results from molecular modeling, Cys-scanning, and domain-swapping studies (Fleishman et al., 2004; Skerrett et al., 2001; Zhou et al., 1997; Kronengold et al., 2003). However, the resolution did not permit side chain placement. The structure indicated that EL1 begins with a 3_{10} helix that transitions to an α-helical conformation. Together EL1 and EL2 form an anti-parallel β-sheet with EL2 stretching over EL1 to form the connexon wall. While X-ray crystallography, EM, and AFM provided significant amounts of information about channel architecture and connexin topology, they were unable to address the structure of the cytoplasmic domains. Protein flexibility, which interferes with these techniques, makes alternative biophysical techniques, such as CD and NMR, ideal tools for studying the cytoplasmic domains.

Cytoplasmic domain structure: NT

The structures of the Cx26NT (M1-K15; Purnick et al., 2000) and Cx32NT (M1-R22; Kalmatsky et al., 2009) domains were determined by solution NMR. Cx26NT residues D2-L10 are helical and residues G11–K15 have a turn-like conformation, whereas the Cx32NT is completely disordered (Figure 3A). The turn-like conformation would allow placement of the Cx26NT domain within the vestibule to act as a voltage sensor. Mutational analysis indicated that G12 is essential for maintaining linker flexibility and retention of voltage-regulated gating. G12 is highly conserved among β-type connexins, suggesting a conserved mechanism regulating GJ channel voltage gating.

CL

To date, the only high-resolution CL structure available is that of the Cx43CL domain (Duffy et al., 2002). The NMR structure of a Cx43CL peptide (D119-K144; Figure 3B) identified residues N122-Q129 and K136-G143 to be helical. Formation of the helices, which depends on acidification, increased the affinity of the CT–CL interaction (Duffy et al., 2002). A mechanism believed to be involved in Cx43 channel closure. Each of the CL helical regions contains a His residue, which is necessary for the helical structure and potentially acts as a pH sensor (Shibayama et al., 2006). Additionally, binding of calmodulin, which causes channel closure, also induces helical structure in the Cx43CL (Zhou et al., 2007).

CT

The structures of the Cx43CT (S255-I382; Figure 3C) and Cx40CT (S251-V351; Figure 3D) were determined by solution NMR (Sorgen et al., 2004; Bouvier et al., 2009). Both domains are primarily disordered; however, the Cx43CT has two short helical regions (A315-T326 and D340-A348 (Sorgen et al., 2004)). The disordered regions are hubs for the binding of proteins involved in GJ regulation and undergo structural transitions upon interaction with

these protein partners (e.g. ZO-1 (Chen et al., 2008); c-Src (Kieken et al., 2009); and tubulin (Saidi Brikci-Nigassa et al., 2012)). The Cx43CT construct S255-I382 has been used often to study channel regulation (e.g. Kieken et al., 2009; Hirst-Jensen et al., 2007; Morley et al., 1996); however, several results indicate that this 'membrane untethered' construct may not be the best model system for structural studies. For example, the EM study by Unger et al. (1999) suggested that residues S255–T263 were helical; however, the NMR structure indicated this region to be flexible and unstructured (Figure 4). Also, not all of the expected Nuclear Overhauser Effects (NOEs) were observed in the two helical regions. The increased flexibility could disrupt structural stability along the CT, interfere with molecular binding, and/or inhibit structural transitions associated with various regulatory events. Therefore, expression, purification, and solution conditions for CD and NMR were optimized for a more native-like construct: the Cx43CT attached to the 4 th TM domain (TM4-Cx43CT) solubilized in detergent micelles (Kellezi et al., 2008; Grosely et al., 2010). At pH 7.5, the TM4-Cx43CT is 33% helical compared to 5% for the soluble Cx43CT. Given that the TM4 portion accounts for 15% of the protein, the data suggest that tethering of the CT domain stabilizes helices extending out from the membrane and/or induces additional structure along portions of the CT. At pH 5.8, the helical content of the TM4-Cx43CT increases to 46%. However, little-to-no difference was observed in the CD spectra of soluble Cx43CT upon acidification, indicating that tethering is required for pH-mediated structural changes in the CT domain.

The NMR backbone assignments and predicted secondary structure of the TM4-Cx43CT have been reported (Grosely et al., 2012). Seven helical regions were predicted along the CT (H1–H7; Figure 4). H1–H3 are consistent with previous EM studies that projected the helical conformation of the TM4 to extend beyond the membrane into the Cx43CT. Additionally, H1 and H2 overlap with a Cx43CT peptide (K234-D259), which adopts a helical conformation upon binding to tubulin (Saidi Brikci-Nigassa et al., 2012), and the two helical domains identified in the soluble Cx43CT are contained within H4 and H5 (Sorgen et al., 2004). The seven CT helices and the helical TM4 (30% and 15% of the TM4-Cx43CT construct, respectively) are consistent with the total helical content of the TM4-Cx43CT observed by CD (Grosely et al., 2010). The ^{15}N-NOESY data suggest that these helical regions are dynamic, as not all expected NOEs were apparent.

Phosphorylation is also implicated in regulating GJs; unfortunately, a complete understanding of the mechanisms by which phosphorylation exerts its effects is lacking. Our laboratory has used CD and NMR to characterize the global and local effects of phosphorylation on the secondary structure and backbone dynamics of the soluble Cx43CT and TM4-Cx43CT (unpublished data). Phospho-mimetic isoforms, which have Asp substitutions at specific Ser/Tyr sites, revealed that phosphorylation can alter the helical content of the Cx43CT, but only when tethered to the membrane. The changes in TM4-Cx43CT helical content were due to alterations in backbone flexibility and conformational preference of the Cx43CT for either helical or random coil structure. The results suggest, in addition to a phosphate being *directly* involved in regulating GJIC (i.e. mediating protein-partner interactions), that phosphorylation could also *indirectly* regulate channel communication. Phosphorylation affected residues adjacent and distal to the site(s) of modification, indicating that the effects propagate along the Cx43CT domain. Phosphorylation of the CT domain could alter channel permeability by *indirectly* modulating the orientation of the transmembrane α-helices, thereby influencing pore size and/or *indirectly* affecting the binding affinity of regulatory molecular interactions through phosphorylation-mediated changes in the conformational preference of the Cx43CT domain.

Since the initial observations of Robertson in 1961, major advancements have been made in our understanding of GJ function and structure. GJs play an essential role in enabling the

propagation and/or amplification of signaling cascades involved in cell growth, development, and whole-organ responses. Numerous diseases and developmental abnormalities including neurodegenerative disorders, skin diseases, and hearing impairment are associated with GJ dysfunction (Dobrowolski & Willecke, 2009). Characterizing the GJ structure has faced several challenges, some of which are inherent to membrane proteins (e.g. protein expression, purification, yield, solubility and crystallization). Overcoming these difficulties has not only led to advancements in the GJ field, but has also driven technological development and progress in the field of protein structure. However, even with an amalgamation of GJ structural information, many questions remain. For example, what are the structural consequences of GJ heteromeric and hetorotypic associations? How do various cellular conditions and posttranslational modifications alter channel structure and regulate channel gating? Consider the functional opposition of Cx43 phosphorylation at S365 and S368. Although in proximity and ~100 Å away from the pore, phosphorylation of S368 results in Cx43 channel closure, whereas phosphorylation at S365 increases GJIC and acts as a gatekeeper by blocking S368 phosphorylation-induced closure (Solan et al., 2007). Future structural studies, in which both the channel and cytoplasmic domains are atomically resolved together, will help address these and other remaining questions about the molecular mechanism(s) regulating GJ channel function and contribute to the eventual development of drugs and therapeutics designed to modulate dysfunctional GJIC.

Acknowledgments

The authors thank Gaelle Spagnol for critically reading the review.

This work is funded by the United States Public Health Service Grant, GM072631. Rosslyn Grosely is funded by the Graduate Assistance in Areas of National Need (GAANN) Fellowship, McDonald Fellowship, Regents Tuitions Fellowship, and the Fred W. Upson Grant.

This work was supported by the United States Public Health Service Grant GM072631.

References

Benedetti EL, Emmelot P. Electron microscopic observations on negatively stained plasma membranes isolated from rat liver. J Cell Biol. 1965; 26:299–305. [PubMed: 4159381]

Benedetti EL, Emmelot P. Hexagonal array of subunits in tight junctions separated from isolated rat liver plasma membranes. J Cell Biol. 1968; 38:15–24. [PubMed: 5691971]

Bennett MV, Aljure E, Nakajima Y, Pappas GD. Electrotonic junctions between teleost spinal neurons: electrophysiology and ultrastructure. Science. 1963; 141:262–264. [PubMed: 13967485]

Beyer EC, Paul DL, Goodenough DA. Connexin43: a protein from rat heart homologous to a gap junction protein from liver. J Cell Biol. 1987; 105:2621–2629. [PubMed: 2826492]

Bouvier D, Spagnol G, Chenavas S, Kieken F, Vitrac H, Brownell S, Kellezi A, Forge V, Sorgen PL. Characterization of the structure and intermolecular interactions between the connexin40 and connexin43 carboxyl-terminal and cytoplasmic loop domains. J Biol Chem. 2009; 284:34257–34271. [PubMed: 19808665]

Cascio M, Gogol E, Wallace BA. The secondary structure of gap junctions. Influence of isolation methods and proteolysis. J Biol Chem. 1990; 265:2358–2364. [PubMed: 1688853]

Caspar DL, Goodenough DA, Makowski L, Phillips WC. Gap junction structures. I. Correlated electron microscopy and x-ray diffraction. J Cell Biol. 1977; 74:605–628. [PubMed: 885916]

Chen J, Pan L, Wei Z, Zhao Y, Zhang M. Domain-swapped dimerization of ZO-1 PDZ2 generates specific and regulatory connexin43-binding sites. EMBO J. 2008; 27:2113–2123. [PubMed: 18636092]

Cheng A, Schweissinger D, Dawood F, Kumar N, Yeager M. Projection structure of full length connexin 43 by electron cryo-crystallography. Cell Commun Adhes. 2003; 10:187–191. [PubMed: 14681014]

Dewey MM, Barr L. Intercellular connection between smooth muscle cells: the nexus. Science. 1962; 137:670–672.10.1126/science.137.3531.670-a [PubMed: 17770946]

Dobrowolski R, Willecke K. Connexin-caused genetic diseases and corresponding mouse models. Antioxid Redox Signal. 2009; 11:283–295. [PubMed: 18831677]

Duffy HS, Sorgen PL, Girvin ME, O'Donnell P, Coombs W, Taffet SM, Delmar M, Spray DC. pH-dependent intramolecular binding and structure involving Cx43 cytoplasmic domains. J Biol Chem. 2002; 277:36706–36714. [PubMed: 12151412]

el Aoumari A, Dupont E, Fromaget C, Jarry T, Briand JP, Kreitman B, Gros D. Immunolocalization of an extracellular domain of connexin43 in rat heart gap junctions. Eur J Cell Biol. 1991; 56:391–400. [PubMed: 1724962]

Farquhar MG, Palade GE. Junctional complexes in various epithelia. J Cell Biol. 1963; 17:375–412. [PubMed: 13944428]

Fernandez Moran H, Oda T, Blair PV, Green DE. A macromolecular repeating unit of mitochondrial structure and function. Correlated electron microscopic and biochemical studies of isolated mitochondria and submitochondrial particles of beef heart muscle. J Cell Biol. 1964; 22:63–100. [PubMed: 14195622]

Fleishman SJ, Unger VM, Yeager M, Ben-Tal N. A Calpha model for the transmembrane alpha helices of gap junction intercellular channels. Mol Cell. 2004; 15:879–888.10.1016/j.molcel.2004.08.016 [PubMed: 15383278]

Gimlich RL, Kumar NM, Gilula NB. Differential regulation of the levels of three gap junction mRNAs in Xenopus embryos. J Cell Biol. 1990; 110:597–605. [PubMed: 2155241]

Goodenough DA. Bulk isolation of mouse hepatocyte gap junctions. Characterization of the principal protein, connexin. J Cell Biol. 1974; 61:557–563. [PubMed: 4363961]

Goodenough, DA. Methods in Membrane Biology. Vol. III. New York: Plenum Publishing Corp; 1975. Methods for the Isolation and Structural Characterization of Hepatocyte Gap Junctions.

Goodenough DA. In vitro formation of gap junction vesicles. J Cell Biol. 1976; 68:220–231. [PubMed: 54358]

Goodenough DA, Stoeckenius W. The isolation of mouse hepatocyte gap junctions. Preliminary chemical characterization and x-ray diffraction. J Cell Biol. 1972; 54:646–656. [PubMed: 4339819]

Grosely R, Kieken F, Sorgen PL. Optimizing the solution conditions to solve the structure of the Connexin43 carboxyl terminus attached to the 4(th) transmembrane domain in detergent micelles. Cell Commun Adhes. 2010; 17:23–33. [PubMed: 20513204]

Grosely R, Kieken F, Sorgen PL. 1H, 13C, and 15N Backbone resonance assignments of the Connexin43 carboxyl terminal domain attached to the 4th transmembrane domain in detergent micelles. J Biomol NMR Assig. 2012 in press.

Hirst-Jensen BJ, Sahoo P, Kieken F, Delmar M, Sorgen PL. Characterization of the pH-dependent interaction between the gap junction protein connexin43 carboxyl terminus and cytoplasmic loop domains. J Biol Chem. 2007; 282:5801–5813. [PubMed: 17178730]

Hoh JH, Lal R, John SA, Revel JP, Arnsdorf MF. Atomic force microscopy and dissection of gap junctions. Science. 1991; 253:1405–1408. [PubMed: 1910206]

Hoh JH, Sosinsky GE, Revel JP, Hansma PK. Structure of the extracellular surface of the gap junction by atomic force microscopy. Biophys J. 1993; 65:149–163.10.1016/S0006-3495(93)81074-9 [PubMed: 8396452]

Kalmatsky BD, Bhagan S, Tang Q, Bargiello TA, Dowd TL. Structural studies of the N-terminus of Connexin 32 using 1H NMR spectroscopy. Arch Biochem Biophys. 2009; 490:9–16. Image reprinted with permission from Elsevier. 10.1016/j.abb.2009.07.015 [PubMed: 19638273]

Karrer HE. The striated musculature of blood vessels. II. Cell interconnections and cell surface. J Biophys Biochem Cytol. 1960; 8:135–150. [PubMed: 13751592]

Kellezi A, Grosely R, Kieken F, Borgstahl GE, Sorgen PL. Purification and reconstitution of the connexin43 carboxyl terminus attached to the 4th transmembrane domain in detergent micelles. Protein Expr Purif. 2008; 59:215–222. [PubMed: 18411056]

Kieken F, Mutsaers N, Dolmatova E, Virgil K, Wit AL, Kellezi A, Hirst-Jensen BJ, Duffy HS, Sorgen PL. Structural and molecular mechanisms of gap junction remodeling in epicardial border zone myocytes following myocardial infarction. Circ Res. 2009; 104:1103–1112. [PubMed: 19342602]

Kronengold J, Trexler EB, Bukauskas FF, Bargiello TA, Verselis VK. Single-channel SCAM identifies pore-lining residues in the first extracellular loop and first transmembrane domains of Cx46 hemichannels. J Gen Physiol. 2003; 122:389–405.10.1085/jgp.200308861 [PubMed: 12975451]

Kumar NM, Gilula NB. Cloning and characterization of human and rat liver cDNAs coding for a gap junction protein. J Cell Biol. 1986; 103:767–776. [PubMed: 2875078]

Lal R, John SA, Laird DW, Arnsdorf MF. Heart gap junction preparations reveal hemiplaques by atomic force microscopy. Am J Physiol. 1995; 268:C968–977. [PubMed: 7733245]

Liu F, Arce FT, Ramachandran S, Lal R. Nanomechanics of hemichannel conformations: connexin flexibility underlying channel opening and closing. J Biol Chem. 2006; 281:23207–23217.10.1074/jbc.M605048200 [PubMed: 16769719]

Loewenstein WR, Kanno Y. Intercellular communication and the control of tissue growth: lack of communication between cancer cells. Nature. 1966; 209:1248–1249. [PubMed: 5956321]

Maeda S, Nakagawa S, Suga M, Yamashita E, Oshima A, Fujiyoshi Y, Tsukihara T. Structure of the connexin 26 gap junction channel at 3.5 A resolution. Nature. 2009; 458:597–602. Image reprinted with permission from Nature Publishing Group. [PubMed: 19340074]

Makowski L, Caspar DL, Phillips WC, Goodenough DA. Gap junction structures. II. Analysis of the x-ray diffraction data. J Cell Biol. 1977; 74:629–645. [PubMed: 889612]

Makowski L, Caspar DL, Phillips WC, Goodenough DA. Gap junction structures. V. Structural chemistry inferred from X-ray diffraction measurements on sucrose accessibility and trypsin susceptibility. J Mol Biol. 1984; 174:449–481. [PubMed: 6716484]

McNutt NS, Weinstein RS. The ultrastructure of the nexus. A correlated thin-section and freeze-cleave study. J Cell Biol. 1970; 47:666–688. [PubMed: 5531667]

Morley GE, Taffet SM, Delmar M. Intramolecular interactions mediate pH regulation of connexin43 channels. Biophys J. 1996; 70:1294–1302. [PubMed: 8785285]

Muller DJ, Hand GM, Engel A, Sosinsky GE. Conformational changes in surface structures of isolated connexin 26 gap junctions. EMBO J. 2002; 21:3598–3607.10.1093/emboj/cdf365 [PubMed: 12110573]

Nicholson BJ, Gros DB, Kent SB, Hood LE, Revel JP. The Mr 28,000 gap junction proteins from rat heart and liver are different but related. J Biol Chem. 1985; 260:6514–6517. [PubMed: 2987225]

Oshima A, Tani K, Hiroaki Y, Fujiyoshi Y, Sosinsky GE. Three-dimensional structure of a human connexin26 gap junction channel reveals a plug in the vestibule. Proc Natl Acad Sci U S A. 2007; 104:10034–10039. [PubMed: 17551008]

Oshima A, Tani K, Hiroaki Y, Fujiyoshi Y, Sosinsky GE. ProjectionstructureofaN-terminaldeletionmutantofconnexin 26 channel with decreased central pore density. Cell Commun Adhes. 2008; 15:85–93.10.1080/15419060802013588 [PubMed: 18649181]

Oshima A, Tani K, Toloue MM, Hiroaki Y, Smock A, Inukai S, Cone A, Nicholson BJ, Sosinsky GE, Fujiyoshi Y. Asymmetric configurations and N-terminal rearrangements in connexin26 gap junction channels. J Mol Biol. 2011; 405:724–735.10.1016/j.jmb.2010.10.032 [PubMed: 21094651]

Paul DL. Molecular cloning of cDNA for rat liver gap junction protein. J Cell Biol. 1986; 103:123–134. [PubMed: 3013898]

Payton BW, Bennett MV, Pappas GD. Permeability and structure of junctional membranes at an electrotonic synapse. Science. 1969; 166:1641–1643. [PubMed: 5360587]

Peracchia C, Dulhunty AF. Low resistance junctions in crayfish. Structural changes with functional uncoupling. J Cell Biol. 1976; 70:419–439. [PubMed: 820701]

Purnick PE, Benjamin DC, Verselis VK, Bargiello TA, Dowd TL. Structure of the amino terminus of a gap junction protein. Arch Biochem Biophys. 2000; 381:181–190. Image reprinted with permission from Elsevier. 10.1006/abbi.2000.1989 [PubMed: 11032405]

Revel JP, Karnovsky MJ. Hexagonal array of subunits in intercellular junctions of the mouse heart and liver. J Cell Biol. 1967; 33:C7–C12. [PubMed: 6036535]

Robertson JD. Ultrastructure of excitable membranes and the crayfish median-giant synapse. Ann N Y Acad Sci. 1961; 94:339–389. [PubMed: 13742210]

Robertson JD. The occurrence of a subunit pattern in the unit membranes of club endings in mauthner cell synapses in goldfish brains. J Cell Biol. 1963; 19:201–221. [PubMed: 14069795]

Saidi Brikci-Nigassa A, Clement MJ, Ha-Duong T, Adjadj E, Ziani L, Pastre D, Curmi PA, Savarin P. Phosphorylation controls the interaction of the connexin43 C-terminal domain with tubulin and microtubules. Biochemistry. 2012; 51:4331–4342.10.1021/bi201806j [PubMed: 22558917]

Shibayama J, Gutierrez C, Gonzalez D, Kieken F, Seki A, Carrion JR, Sorgen PL, Taffet SM, Barrio LC, Delmar M. Effect of charge substitutions at residue his-142 on voltage gating of connexin43 channels. Biophys J. 2006; 91:4054–4063. [PubMed: 16963503]

Sjostrand FS, Andersson-Cedergren E, Dewey MM. The ultrastructure of the intercalated discs of frog, mouse and guinea pig cardiac muscle. J Ultrastruct Res. 1958; 1:271–287. [PubMed: 13550367]

Skerrett M, Kasperek E, Cao FL, Shin JH, Aronowitz J, Ahmed S, Nicholson BJ. Application of SCAM (substituted cysteine accessibility method) to gap junction intercellular channels. Cell Commun Adhes. 2001; 8:179–185. [PubMed: 12064585]

Solan JL, Marquez-Rosado L, Sorgen PL, Thornton PJ, Gafken PR, Lampe PD. Phosphorylation at S365 is a gatekeeper event that changes the structure of Cx43 and prevents down-regulation by PKC. J Cell Biol. 2007; 179:1301–1309. [PubMed: 18086922]

Sorgen PL, Duffy HS, Sahoo P, Coombs W, Delmar M, Spray DC. Structural changes in the carboxyl terminus of the gap junction protein connexin43 indicates signaling between binding domains for c-Src and zonula occludens-1. J Biol Chem. 2004; 279:54695–54701. [PubMed: 15492000]

Stoeckenius W. Some electron microscopical observations on liquid-crystalline phases in lipid-water systems. J Cell Biol. 1962; 12:221–229. [PubMed: 13917314]

Thimm J, Mechler A, Lin H, Rhee S, Lal R. Calcium-dependent open/closed conformations and interfacial energy maps of reconstituted hemichannels. J Biol Chem. 2005; 280:10646–10654.10.1074/jbc.M412749200 [PubMed: 15615707]

Tibbitts TT, Caspar DL, Phillips WC, Goodenough DA. Diffraction diagnosis of protein folding in gap junction connexons. Biophys J. 1990; 57:1025–1036.10.1016/S0006-3495(90)82621-7 [PubMed: 2160297]

Unger VM, Kumar NM, Gilula NB, Yeager M. Three-dimensional structure of a recombinant gap junction membrane channel. Science. 1999; 283:1176–1180. Image reprinted with permission from AAAS. [PubMed: 10024245]

Unwin PN, Ennis PD. Two configurations of a channel-forming membrane protein. Nature. 1984; 307:609–613. [PubMed: 6320017]

Verselis VK, Trelles MP, Rubinos C, Bargiello TA, Srinivas M. Loop gating of connexin hemichannels involves movement of pore-lining residues in the first extracellular loop domain. J Biol Chem. 2009; 284:4484–4493.10.1074/jbc.M807430200 [PubMed: 19074140]

Yu J, Bippes CA, Hand GM, Muller DJ, Sosinsky GE. Aminosulfonate modulated pH-induced conformational changes in connexin26 hemichannels. J Biol Chem. 2007; 282:8895–8904.10.1074/jbc.M609317200 [PubMed: 17227765]

Zampighi G, Unwin PN. Two forms of isolated gap junctions. J Mol Biol. 1979; 135:451–464. [PubMed: 537084]

Zhou XW, Pfahnl A, Werner R, Hudder A, Llanes A, Luebke A, Dahl G. Identification of a pore lining segment in gap junction hemichannels. Biophys J. 1997; 72:1946–1953.10.1016/S0006-3495(97)78840-4 [PubMed: 9129799]

Zhou Y, Yang W, Lurtz MM, Ye Y, Huang Y, Lee HW, Chen Y, Louis CF, Yang JJ. Identification of the calmodulin binding domain of connexin 43. J Biol Chem. 2007; 282:35005–35017.10.1074/jbc.M707728200 [PubMed: 17901047]

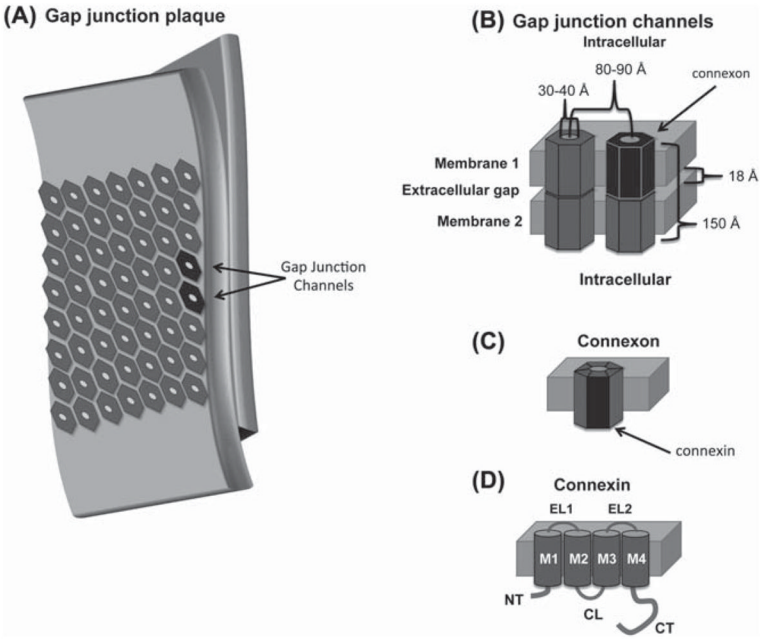

Figure 1.

Cartoon depiction of a (A) gap junction plaque, (B) gap junction channel, (C) connexon, and (D) connexin. A subunit from each structure is highlighted in black. Abbreviations are as follows: NT, amino terminus domain; TM, transmembrane 1–4; EL, extracellular loop 1 and 2; CL, cytoplasmic loop; CT carboxyl terminus domain.

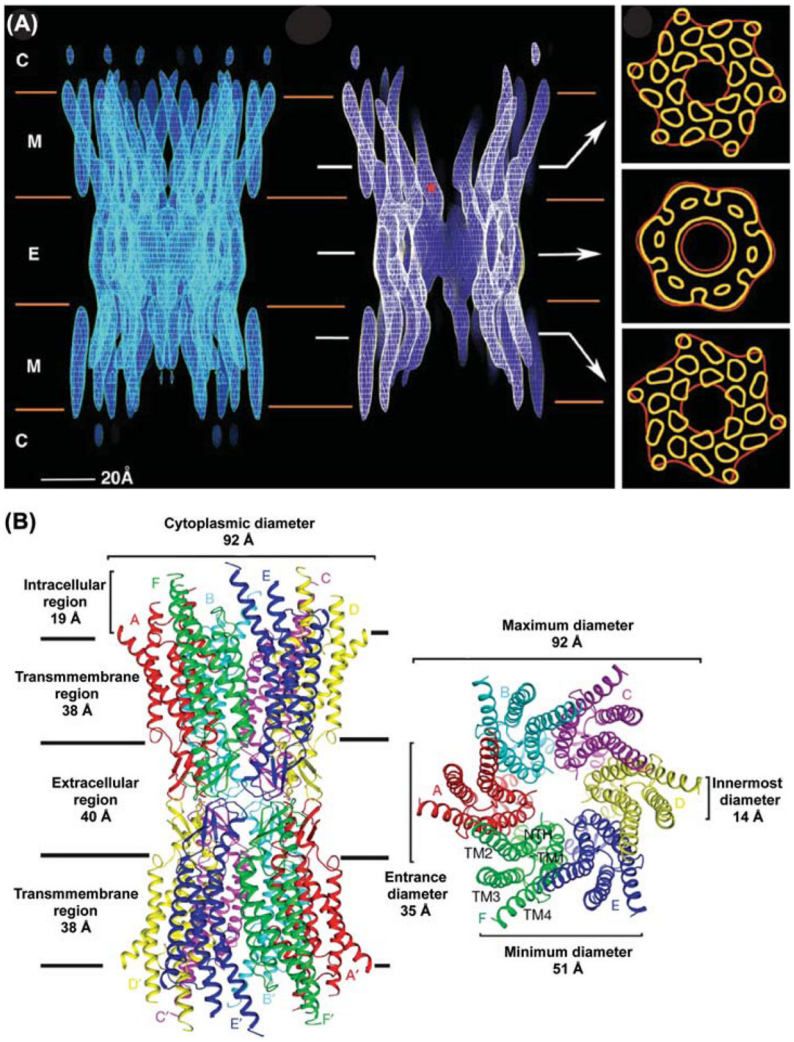

Figure 2.

Structure of a gap junction channel. (A) Cryo-EM images of a Cx43 channel truncated at T263. The left panel is a full side view of the channel. In the middle image, electron density has been cropped to reveal channel interior. The cytoplasmic (C), membrane (M), and extracellular (E) boundaries are indicated. The asterisk (*) is located at the narrowest point within the intercellular channel. Arrows indicate the area from which the cross sections shown on the right were taken. Tubular densities in the top and bottom sections of the right panel are from the 24 α-helical transmembrane domains. The density in the middle section is from the six connexins that comprise a hexameric connexon. *Image is reprinted with permission from (*Unger et al., 1999). (B) Ribbon diagram of the Cx26 gap junction channel X-ray crystal structure. The channel dimensions are provided in the side view (left) and top view (right) of the channel. The transmembrane domains (TM1–4) and connexins (A–F) are indicated. *Image is reprinted with permission (*Maeda et al., 2009).

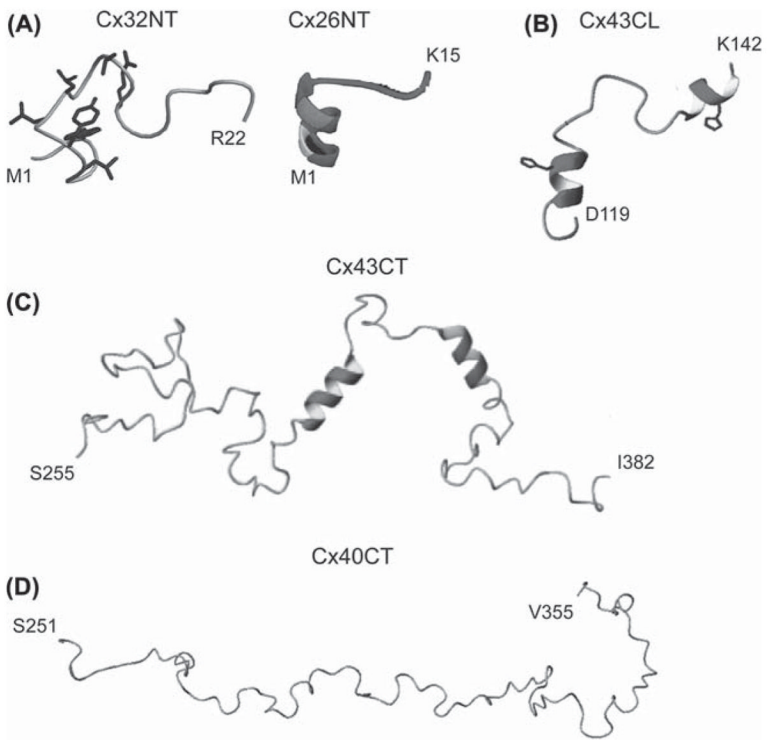

Figure 3.

Structure of connexin cytoplasmic domains. Solution NMR structures for the (A) Cx32 and Cx26 NT domains, (B) Cx43CL domain, (C) Cx43CT domain and (D) Cx40CT domain. Helical regions are indicated by the ribbon diagrams. *Images are reprinted with permission: Cx32,* Kalmatsky et al., 2009; *Cx26* Purnick et al., 2000; *Cx43CL2,* Duffy et al., 2002; *Cx43CT,* Sorgen et al., 2004; *Cx40CT* Bouvier et al., 2009.

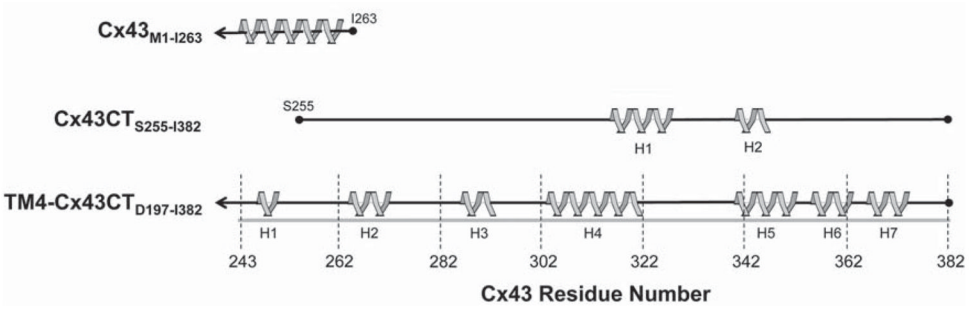

Figure 4.

Comparison of Cx43CT sequences used for structural structures. Helical regions (gray ribbons) of the Cx43CT predicted from crystallographic (Cx43) and NMR (TM4-Cx43CT) data are depicted. Also shown are the helical domains identified from the solution structure of the soluble Cx43CT domain for comparison. The gray line represents the length of the full Cx43CT domain and the black lines indicate the protein sequence used in each study.